Journal of Physics:
Condensed Matter

PURPOSE-LED PUBLISHING™

PAPER • **OPEN ACCESS**

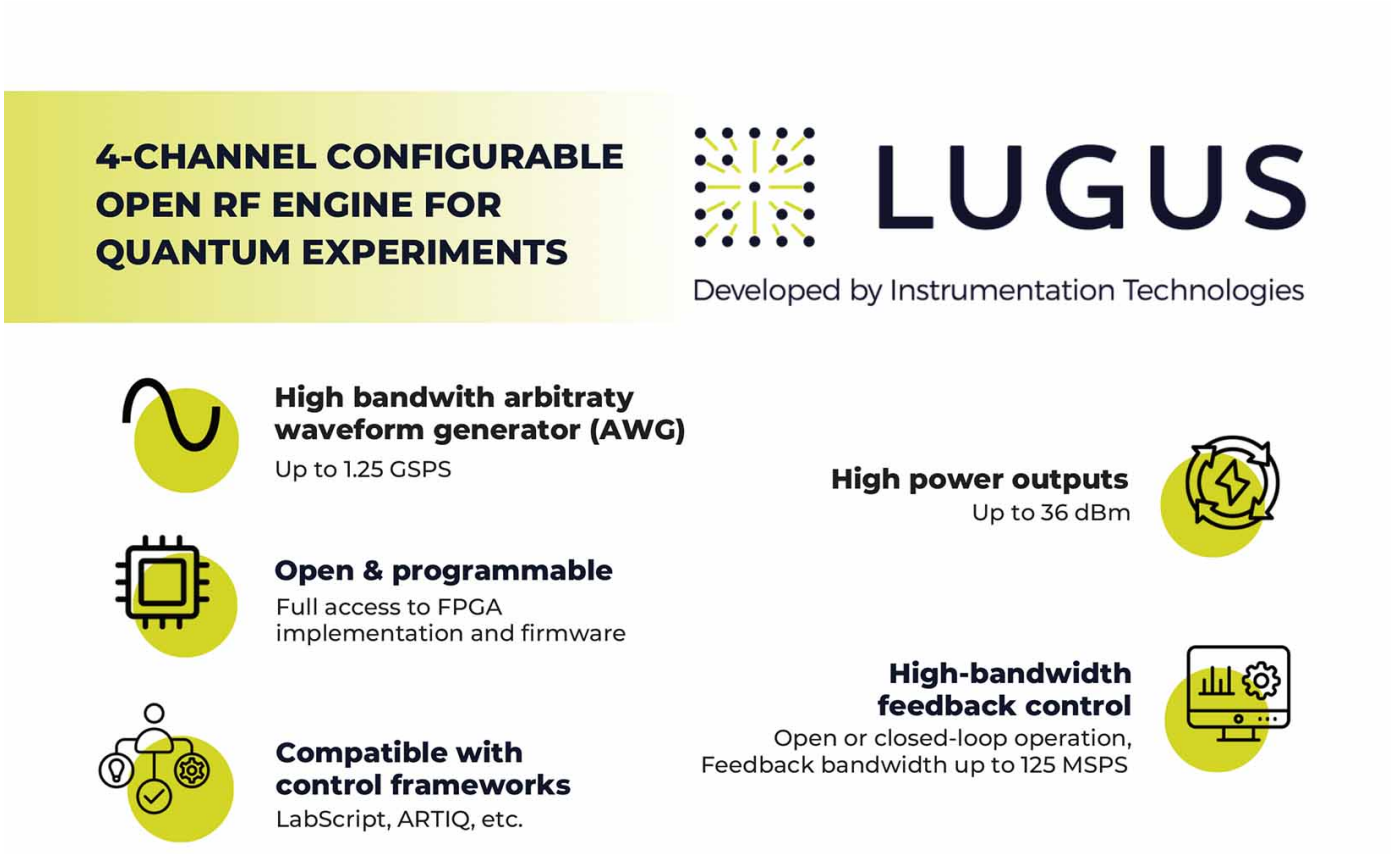
Stress calculation in linear scaling DFT: convergence and dynamics

To cite this article: Shereif Y Mujahed *et al* 2026 *J. Phys.: Condens. Matter* **38** 425501

View the article online for updates and enhancements.

You may also like

- Introductory Remarks: Linear Scaling Methods
D R Bowler, J-L Fattebert, M J Gillan et al.
- A localized-basis scheme for molecular dynamics
Z Lin and J Harris
- Linear-scaling first-principles molecular dynamics of complex biological systems with the Conquest code
Takao Otsuka, Makoto Taiji, David R. Bowler et al.



This content was downloaded from IP address 144.213.253.16 on 21/10/2026 at 02:28

Journal of Physics: Condensed Matter

Check for updates

OPEN ACCESS

RECEIVED
8 July 2026

REVISED
24 September 2026

ACCEPTED FOR PUBLICATION
30 September 2026

PUBLISHED
20 October 2026

Original content from this work may be used under the terms of the Creative Commons Attribution 4.0 licence.

Any further distribution of this work must maintain attribution to the author(s) and the title of the work, journal citation and DOI.

PAPER

Stress calculation in linear scaling DFT: convergence and dynamics

Shereif Y Mujahed[1,2], **Tsuyoshi Miyazaki**[3] and **David R Bowler**[1,2,3,*]

[1] Dept. Physics & Astronomy, University College London, Gower Street, London, WC1E 6BT, United Kingdom
[2] London Centre for Nanotechnology, University College London, 17–19 Gordon Street, London, WC1H 0AH, United Kingdom
[3] Research Centre for Materials Nanoarchitectonics (WPI-MANA), National Institute for Materials Science (NIMS), 1–1 Namiki, Tsukuba, Ibaraki 305-0044, Japan
[*] Author to whom any correspondence should be addressed.

E-mail: david.bowler@ucl.ac.uk

Keywords: stress, linear scaling, molecular dynamics

Abstract

We present the approach needed to calculate stress within density functional theory (DFT) using a localized orbital basis, both for exact diagonalisation and linear scaling approaches, and demonstrate our implementation within the large scale DFT code CONQUEST. For the linear scaling approach, we test the rate of convergence of stress with density matrix range, and compare it to the convergence of energy and forces for different materials with a range of band gaps. We show that excellent convergence is found for modest cutoffs (below 0.1 GPa error for range of 20 a_0), and show that large-scale isothermal-isobaric molecular dynamics is stable and accurate, showing negligible drift over picoseconds of dynamics.

1. Introduction

Density functional theory (DFT) has become the method of choice for electronic structure calculations [1]. In condensed matter research, plane wave basis sets have often been the basis of choice, which has tended to limit the size of all but the largest simulations to hundreds of atoms [2]; the adoption of local orbital basis sets has enabled larger scale simulations, both with exact diagonalisation and with linear scaling methods to find the ground state [3–7]. The CONQUEST code [7] has demonstrated simulations of several thousand atoms with exact diagonalisation [8], and millions of atoms with linear scaling [9, 10].

Simulations of condensed and soft matter systems require that the forces on the ions can be efficiently calculated as exact differentials of the energy; in many cases, the stresses on the simulation cell are also required. We have discussed the calculation of forces in CONQUEST for both exact diagonalisation and linear scaling before [11], and noted that the motion of basis functions with the ions requires evaluation of Pulay terms [12] which are readily found analytically. The evaluation of stresses is standard in plane-wave DFT [1] though for plane-wave basis set there is a missing term which arises from the change of basis with simulation cell size (a Pulay stress), and cannot be calculated analytically, leading to a need to increase basis set size for stress evaluation. The calculation of stress for local orbital basis sets has been shown before [13, 14] but the calculation of stress with linear scaling, and the convergence of the stress, has only been investigated in the context of finite electronic temperature simulations [15]. We reported preliminary results [7] on stress with linear scaling methods, but gave only an overview of the approach; below, we give full details, and note an important correction to our preliminary results. We also demonstrate stable NPT molecular dynamics.

The paper is organized as follows. We recap the expressions required to evaluate the energy both in exact diagonalisation and linear scaling modes; we note an important constraint that is applied to maintain electron number in linear scaling calculations. We then examine the approach needed to calculate stresses with localized orbitals and the linear scaling approach in CONQUEST. We conclude by presenting various tests of the implementation; first, testing the convergence of energy, forces and stresses with density matrix range, and then demonstrating stable molecular dynamics in different ensembles.

© 2026 The Author(s). Published by IOP Publishing Ltd

2. Energies

For a system with total energy E we define the forces on the atoms and the stresses on the simulation cell in the usual way, with $\mathbf{F}_i = -\nabla_i E$ for atom i, and $\sigma_{\lambda\mu} = (1/\Omega)\partial E/\partial\epsilon_{\lambda\mu}$, for the strain $\epsilon_{\lambda\mu}$ (with λ and μ each representing one of x, y or z) and Ω the simulation cell volume. This definition of stress has units of pressure; an alternative definition, often known as the internal stress, omits the prefactor of $1/\Omega$ to give units of energy [16, 17].

In order to implement accurate forces and stresses, we have to consider the details of how energies are calculated, and ensure that the forces and stresses are exact derivatives of the energy. In CONQUEST, in common with other local orbital pseudopotential codes such as Siesta [14] and OpenMX [18], we use a reformulation of the electrostatic part of the total energy based on neutral atom charges. By associating a pseudo-atomic density (PAD) $n_i^{(a)}(\mathbf{r})$ with each atom [19], we can rewrite the Hartree energy of the electrons and the ionic core–core energy, avoiding any long range terms, leaving only a screened core-core interation (SCC). We combine the local part of the pseudopotential and the Hartree potential from the PAD to give a neutral atom potential: $V_{\mathrm{NA}}(\mathbf{r}) = \sum_i V_{\mathrm{PS,Loc},i}(\mathbf{r}) + V^{(a)}_{\mathrm{Ha},i}(\mathbf{r})$. We define the total PAD for the system as $n^{\mathrm{PAD}}(\mathbf{r}) = \sum_i n_i^{(a)}(\mathbf{r})$, and a charge density difference between the ground state charge density and the PAD as $\delta n(\mathbf{r}) = n(\mathbf{r}) - n^{\mathrm{PAD}}(\mathbf{r})$. This density difference gives a potential $V_{\delta\mathrm{Ha}}$ and an energy $E_{\delta\mathrm{Ha}}$, and we define the Harris–Foulkes [20, 21] and Kohn–Sham (KS) [22] energies below in equations (2) and (4), with a Hamiltonian written as:

$$\hat{H} = \left(-\frac{1}{2}\nabla^2 + \hat{V}_{\mathrm{NA}} + \hat{V}_{\mathrm{PS,NL}} + V_{\delta\mathrm{Ha}} + V_{\mathrm{XC}}\right) \tag{1}$$

where $\hat{V}_{\mathrm{PS,NL}}$ is the non-local part of the pseudopotential.

CONQUEST uses a basis set of localized functions, known as support functions [23], to represent the KS eigenstates. Most commonly these functions are represented by pseudo-atomic orbitals (PAOs) which are generated by solving the Schrödinger equation for isolated atoms, using pseudopotentials [24]. The eigenstates are then expressed as: $|\psi_n\rangle = \sum_{i\alpha} c_n^{i\alpha}|\phi_{i\alpha}\rangle$, where $i\alpha$ indicates the support functions on atom i, with the support functions indexed by α. Using these basis functions, the Schrödinger equation can be re-written as a matrix equation, $H_{i\alpha j\beta}c_n^{j\beta} = \epsilon_n S_{i\alpha j\beta}c_n^{j\beta}$, noting that the support functions are non-orthogonal, with overlap matrix $S_{i\alpha j\beta}$, and the matrices defined in the usual way: $H_{i\alpha j\beta} = \langle\phi_{i\alpha}|\hat{H}|\phi_{j\beta}\rangle$ and $S_{i\alpha,j\beta} = \langle\phi_{i\alpha}|\phi_{j\beta}\rangle$. The individual terms in the energy can be defined either in terms of the eigenvalues and eigenstates, or in terms of the Hamiltonian and density matrices; the latter approach, coupled with sparse matrices, enables a linear scaling formulation of DFT to be constructed [25, 26].

2.1. Energy in terms of eigenvalues and eigenstates

We present first the Harris–Foulkes (HF) and KS energies used when solving by diagonalisation; below we turn to the linear scaling formulation. We also consider the inclusion of non-linear partial core corrections (PCC) [27] which include an additional charge density in the core region of each atom, $n_i^{\mathrm{C}}(\mathbf{r})$, in the calculation of the exchange-correlation energy, and for simplicity we define $\tilde{n}(\mathbf{r}) = n(\mathbf{r}) + n^{\mathrm{C}}(\mathbf{r})$, where $n^{\mathrm{C}}(\mathbf{r}) = \sum_i n_i^{\mathrm{C}}(\mathbf{r})$.

$$E_{\mathrm{HF}} = E_{\mathrm{Band}} + \Delta E_{\mathrm{Ha}} + \Delta E_{\mathrm{XC}} + E_{\mathrm{SCC}} \tag{2}$$

$$E_{\mathrm{HF}} = \sum_n 2f_n\epsilon_n + \left[-\frac{1}{2}\int \mathrm{d}\mathbf{r}\delta V_{\mathrm{Ha}}(\mathbf{r})\,\delta n(\mathbf{r}) - \int \mathrm{d}\mathbf{r}\delta V_{\mathrm{Ha}}(\mathbf{r})\,n^{\mathrm{PAD}}(\mathbf{r})\right] + \int \mathrm{d}\mathbf{r}\left(\tilde{n}(\mathbf{r})\,\epsilon_{\mathrm{XC}}[\tilde{n}(\mathbf{r})] - n(\mathbf{r})\,\mu_{\mathrm{XC}}[\tilde{n}(\mathbf{r})]\right) + \frac{1}{2}\left(\sum_{i,j}\frac{Z_iZ_j}{|\mathbf{R}_i - \mathbf{R}_j|} - \int \mathrm{d}\mathbf{r}V^{(a)}_{\mathrm{Ha},j}(\mathbf{r})\,n_i^{(a)}(\mathbf{r})\right) \tag{3}$$

$$E_{\mathrm{KS}} = E_{\mathrm{KE}} + E_{\mathrm{NA}} + E_{\mathrm{PS,NL}} + E_{\delta Ha} + E_{\mathrm{XC}} + E_{\mathrm{SCC}} \tag{4}$$

$$E_{\mathrm{KS}} = -\frac{1}{2}\sum_{n} 2f_n\langle\psi_n\left|\nabla^2\right|\psi_n\rangle + \int \mathrm{d}\mathbf{r}V_{\mathrm{NA}}(\mathbf{r})\,n(\mathbf{r}) + \sum_{n} 2f_n\langle\psi_n|\hat{V}_{\mathrm{PS,NL}}|\psi_n\rangle + \frac{1}{2}\int \mathrm{d}\mathbf{r}\delta n(\mathbf{r})\,\delta V_{\mathrm{Ha}}(\mathbf{r}) + \int \mathrm{d}\mathbf{r}\tilde{n}(\mathbf{r})\,\epsilon_{\mathrm{XC}}[\tilde{n}(\mathbf{r})] + \frac{1}{2}\left(\sum_{i,j}\frac{Z_iZ_j}{|\mathbf{R}_i-\mathbf{R}_j|} - \int \mathrm{d}\mathbf{r}V^{(a)}_{\mathrm{Ha,j}}(\mathbf{r})\,n^{(a)}_i(\mathbf{r})\right) \tag{5}$$

where ϵ_n are the eigenvalues indexed with subscript n, f_n are the occupancies of the eigenstates and the non-local pseudopotential is defined as $\hat{V}_{\mathrm{PS,NL}} = \sum_i\sum_\gamma |\chi_{i\gamma}\rangle A_\gamma\langle\chi_{i\gamma}|$, summing over atoms i and projectors γ in the usual way [28].

When operating without self-consistency [29], we use the fixed superposition of atomic densities defined above as the density, so that $n(\mathbf{r}) = n^{\mathrm{PAD}}(\mathbf{r})$, which fits well with the neutral-atom approach. In this case, only the HF energy is reliable, and $\Delta E_{\mathrm{Ha}} = 0$ as $\delta n(\mathbf{r}) = 0$, while ΔE_{XC} is found as usual, but with $\tilde{n}(\mathbf{r}) = n^{\mathrm{PAD}}(\mathbf{r}) + n^{\mathrm{C}}(\mathbf{r})$.

2.2. Energy in terms of the density matrix

For linear scaling operation, all calculations are performed in terms of the density matrix and the charge density [9, 30]. The density matrix in real space is defined in terms of the support functions and a matrix $K^{i\alpha j\beta}$ as $\rho(\mathbf{r},\mathbf{r}') = \sum_{i\alpha j\beta}\phi_{i\alpha}(\mathbf{r})K^{i\alpha j\beta}\phi_{j\beta}(\mathbf{r}')$, and the connection to eigenvector coefficients can be seen in the formal definition of $K^{i\alpha j\beta} = \sum_n f_n c_n^{i\alpha\star}c_n^{j\beta}$. The charge density is then written as $n(\mathbf{r}) = \sum_{i\alpha j\beta}\phi_{i\alpha}(\mathbf{r})K^{i\alpha j\beta}\phi_{j\beta}(\mathbf{r})$ and the energies are given by:

$$E_{\mathrm{HF}} = \sum_n 2\mathrm{Tr}[\mathrm{KH}] + \left[-\frac{1}{2}\int \mathrm{d}\mathbf{r}\delta V_{\mathrm{Ha}}(\mathbf{r})\,\delta n(\mathbf{r}) - \int \mathrm{d}\mathbf{r}\delta V_{\mathrm{Ha}}(\mathbf{r})\,n^{\mathrm{PAD}}(\mathbf{r})\right] + \int \mathrm{d}\mathbf{r}\left(\tilde{n}(\mathbf{r})\,\epsilon_{\mathrm{XC}}[\tilde{n}(\mathbf{r})] - n(\mathbf{r})\,\mu_{\mathrm{XC}}[\tilde{n}(\mathbf{r})]\right) + \frac{1}{2}\left(\sum_{i,j}\frac{Z_iZ_j}{|\mathbf{R}_i-\mathbf{R}_j|} - \int \mathrm{d}\mathbf{r}V^{(a)}_{\mathrm{Ha,j}}(\mathbf{r})\,n^{(a)}_i(\mathbf{r})\right) \tag{6}$$

$$E_{\mathrm{KS}} = -\frac{1}{2}\sum_{i\alpha j\beta} 2K^{j\beta i\alpha}\langle\phi_{i\alpha}\left|\nabla^2\right|\phi_{j\beta}\rangle + \int \mathrm{d}\mathbf{r}V_{\mathrm{NA}}(\mathbf{r})\,n(\mathbf{r}) + \sum_{i\alpha j\beta} 2K^{j\beta i\alpha}\langle\phi_{i\alpha}|\hat{V}_{\mathrm{PS,NL}}|\phi_{j\beta}\rangle + \frac{1}{2}\int \mathrm{d}\mathbf{r}\delta n(\mathbf{r})\,\delta V_{\mathrm{Ha}}(\mathbf{r}) + \int \mathrm{d}\mathbf{r}\tilde{n}(\mathbf{r})\,\epsilon_{\mathrm{XC}}[\tilde{n}(\mathbf{r})] + \frac{1}{2}\left(\sum_{i,j}\frac{Z_iZ_j}{|\mathbf{R}_i-\mathbf{R}_j|} - \int \mathrm{d}\mathbf{r}V^{(a)}_{\mathrm{Ha,j}}(\mathbf{r})\,n^{(a)}_i(\mathbf{r})\right) \tag{7}$$

For relatively small systems (up to a few thousand atoms) the ground state is found by direct diagonalisation of the Hamiltonian [7]. To go beyond systems of this size, linear scaling methods are needed [25], as described in the next section.

2.3. Linear scaling and electron number

The ground state density matrix of semiconducting and insulating systems (i.e. systems with a gap) can be found with computational effort that scales linearly with system size [25, 26] by working with localized functions as basis functions, and restricting the range of the density matrix (a controlled approximation). Within CONQUEST, a variational minimization of the energy with respect to the density matrix elements is performed, while maintaining two properties of the system: idempotency of the density matrix; and correct total electron number.

Idempotency is imposed approximately, using the LNV approach [31, 32], where the density matrix K is written in terms of an *auxiliary* density matrix, L, as $K = 3LSL - 2LSLSL$ and the elements of the auxiliary density matrix, $L^{i\alpha j\beta}$, are varied in the search for the ground state. The initial density matrix is constructed using the Palser-Manolopoulos generalization of the McWeeny transform [33, 34].

The electron number is found as $N_{\mathrm{e}}^{(K)} = 2\mathrm{Tr}[\mathrm{KS}]$, where the superscript $^{(K)}$ is used to distinguish the calculated electron number from the desired electron number, N_{e}. To optimize the energy with respect to the elements of the auxiliary density matrix, $L^{i\alpha j\beta}$, while maintaining electron number, we use a Lagrange multiplier, μ, to impose the condition [23]. As above, we have $E_{\mathrm{band}} = 2\mathrm{Tr}[\mathrm{KH}]$, and we define a modified band energy which includes the Lagrange multiplier:

$$\tilde{E}_{\mathrm{band}} = E_{\mathrm{band}} - \mu\left(N_{\mathrm{e}}^{(K)} - N_{\mathrm{e}}\right) \tag{8}$$

$$= 2\mathrm{Tr}[\mathrm{KH}] - \mu\left(2\mathrm{Tr}[\mathrm{KS}] - N_{\mathrm{e}}\right) \tag{9}$$

Naturally, when the density matrix gives the target electron number, this energy is identically equal to the band energy. It is sometimes convenient to define $H' = H - \mu S$ and $\tilde{E}_{\mathrm{band}} = 2\mathrm{Tr}\left[\mathrm{KH}'\right] + \mu N_{\mathrm{e}}$ to include the Lagrange multiplier in the Hamiltonian [23], but this can obscure a contribution to the forces discussed below, and we do not follow this convention.

To find the optimum ground state, we need the derivative of this energy with respect to the auxiliary density matrix elements:

$$\begin{aligned}\frac{\partial \tilde{E}_{\mathrm{band}}}{\partial L} &= \frac{\partial E_{\mathrm{band}}}{\partial L} - \mu \frac{\partial N_{\mathrm{e}}^{(K)}}{\partial L} \\ \frac{\partial \tilde{E}_{\mathrm{band}}}{\partial L} &= \left[6\left(HLS + SLH\right) - 4\left(HLSLS - SLHLS - SLSLH\right)\right] - \mu\left[12\left(SLS - SLSLS\right)\right]. \end{aligned} \tag{10}$$

Here we have defined the change in electron number calculated from the K matrix with respect to the elements of the auxiliary density matrix as $\partial N_{\mathrm{e}}^{(K)}/\partial L$. We can then set the value of the Lagrange multiplier so that, to first order, the electron number is preserved while the energy is minimized. This is imposed by ensuring that the variation in energy is orthogonal to the variation in electron number:

$$\begin{aligned} \frac{\partial \tilde{E}_{\mathrm{band}}}{\partial L} \cdot \frac{\partial N_{\mathrm{e}}^{(K)}}{\partial L} &= 0 \\ \left(\frac{\partial E_{\mathrm{band}}}{\partial L} - \mu \frac{\partial N_{\mathrm{e}}^{(K)}}{\partial L}\right) \cdot \frac{\partial N_{\mathrm{e}}^{(K)}}{\partial L} &= 0 \\ \Rightarrow \left(\frac{\partial E_{\mathrm{band}}}{\partial L} \cdot \frac{\partial N_{\mathrm{e}}^{(K)}}{\partial L}\right) \Big/ \left(\frac{\partial N_{\mathrm{e}}^{(K)}}{\partial L} \cdot \frac{\partial N_{\mathrm{e}}^{(K)}}{\partial L}\right) &= \mu. \end{aligned} \tag{11}$$

Of course, the Lagrange multiplier, μ, is the chemical potential for the electrons.

At the electronic ground state, where $\partial \tilde{E}_{\mathrm{band}}/\partial L = 0$, we can find the contribution to the ionic forces and the stresses from the band energy (and associated Lagrange multiplier term) by considering variations in the energy with respect to the Hamiltonian and overlap matrices [11]:

$$\tilde{E}_{\mathrm{band}} = E_{\mathrm{band}} - \mu\left(N_{\mathrm{e}}^{(K)} - N_{\mathrm{e}}\right) = 2\mathrm{Tr}\left[\mathrm{KH}\right] - \mu\left(2\mathrm{Tr}\left[\mathrm{KS}\right] - N_{\mathrm{e}}\right) \tag{12}$$

$$\delta\tilde{E}_{\mathrm{band}} = \delta E_{\mathrm{band}} - \mu \delta N_{\mathrm{e}}^{(K)} \tag{13}$$

$$\begin{aligned}\delta E_{\mathrm{band}} &= 2\mathrm{Tr}\left[\left(3L\delta SL - 2L\delta SLSL - 2LSL\delta SL\right)H\right] + 2\mathrm{Tr}\left[\left(3LSL - 2LSLSL\right)\delta H\right] \\ &= 2\mathrm{Tr}\left[K\delta H\right] - 2\mathrm{Tr}\left[G\delta S\right] \end{aligned} \tag{14}$$

$$G = 2LHLSL + 2LSLHL - 3LHL \tag{15}$$

$$\begin{aligned}\delta N_{\mathrm{e}}^{(K)} &= 2\mathrm{Tr}\left[\left(3L\delta SL - 2L\delta SLSL - 2LSL\delta SL\right)S\right] + 2\mathrm{Tr}\left[\left(3LSL - 2LSLSL\right)\delta S\right] \\ &= 2\mathrm{Tr}\left[\left(6LSL - 6LSLSL\right)\delta S\right] \end{aligned} \tag{16}$$

$$\delta\tilde{E}_{\mathrm{band}} = 2\mathrm{Tr}\left[K\delta H\right] - 2\mathrm{Tr}\left[G\delta S\right] - 2\mu\mathrm{Tr}\left[\left(6LSL - 6LSLSL\right)\delta S\right] = 2\mathrm{Tr}\left[K\delta H\right] - 2\mathrm{Tr}\left[\tilde{G}\delta S\right] \tag{17}$$

$$\tilde{G} = 2LHLSL + 2LSLHL - 3LHL + \mu\left(6LSL - 6LSLSL\right). \tag{18}$$

The sign of the matrix G is chosen for compatibility with the equivalent matrix required for force and stress calculations with exact diagonalisation:

$$G^{i\alpha j\beta} = \sum_n f_n \epsilon_n c_n^{i\alpha\star} c_n^{j\beta}. \tag{19}$$

It is important to note that in O(N) calculations there is a contribution to the forces and stresses from the variation of the electron number with the overlap matrix which arises from the Lagrange multiplier: the final term in equations (13) and (17). This term makes an almost negligible change to the forces, typically around 1×10^{-4} Ha/a_0, and was neglected in our original formulation of forces [11]; the effect of the term is only visible as a small variation in the energy conservation of NVE molecular dynamics runs [35], and makes no difference to optimized structures. However, the term forms a significant part of the stresses, and must be included for correct agreement between numerical and analytic stresses at small L matrix ranges. As the L matrix range increases, the contribution tends to zero, since the L matrix tends towards perfect idempotency, with $LSL = L$; the small fluctuations in energy over time in NVE MD runs also reduce with increasing density matrix range, and are eliminated when this extra contribution to the force is included.

3. Formulating stress with localized orbitals and linear scaling

We have separated the contributions to the stress into different types, in a similar way to the presentation of forces [11]. Hellmann–Feynman stresses arise from explicit dependence of the potentials on the atom positions via the strain, while Pulay stresses come from the change in the basis when atoms move (since the basis is atom-centered). There are then further miscellaneous stresses which are important but do not fit neatly into any category. We note that the calculation of the stress requires negligible time, as it is included with the force evaluation (this is standard for local orbital codes, in contrast to plane wave basis sets).

3.1. Hellmann–Feynman stress

The Hellmann–Feynman stress is straightforward, and equivalent to other codes, coming from the pseudopotentials; there is an extra contribution from the screened Hartree potential in the neutral atom formulation.

$$\sigma^{\mathrm{HF}}_{\lambda\mu} = \sum_i \int \mathrm{d}\mathbf{r} n(\mathbf{r}) \frac{\partial V_i^{\mathrm{NA}}(\mathbf{r})}{\partial R_{i\lambda}} R_{i\mu} - 2\sum_i \sum_{ab} K_{ab} \langle \phi_a \mid (\nabla_{i\lambda}\chi_b) R_{i\mu} \rangle A_i \langle \chi_i \mid \phi_b \rangle - \sum_i \int \mathrm{d}\mathbf{r} \delta V_{\mathrm{Ha}}(\mathbf{r}) \frac{\partial n_i^{\mathrm{PAD}}}{\partial R_{i\lambda}} R_{i\mu}. \tag{20}$$

To understand why we classify the final term as a Hellmann–Feynman term, we note that the screened Hartree energy is written as $E_{\delta Ha} = \frac{1}{2}\int \mathrm{d}\mathbf{r}\delta V_{\mathrm{Ha}}\left(n(\mathbf{r}) - \sum_i n_i^{\mathrm{PAD}}(\mathbf{r})\right)$, so there is a contribution to the force and stress from the change of $n_i^{\mathrm{PAD}}(\mathbf{r})$ with atomic position. The equivalence to a Hellmann–Feynman force comes because the integral can be recast as $\delta n(\mathbf{r})$ interacting with $V_{\mathrm{Ha}}^{\mathrm{PAD}}(\mathbf{r})$, the potential due to the atomic density.

3.2. Pulay stresses

Following the forces [11], we find that there are two contributions to the Pulay stress, coming from changes in the Hamiltonian and overlap matrices; we term these ϕ-Pulay and S-Pulay stresses, respectively. In equation (21) below, the first three terms form the ϕ-Pulay stress (contributions from the local potentials, i.e. neutral atom, Hartree and XC potentials, in the first term; the kinetic energy in the second term; and the non-local potential in the third term) while the fourth contribution forms the S-Pulay stress.

$$\sigma^{\mathrm{Pulay}}_{\lambda\mu} = -4\sum_i \sum_{ab} K_{ab} \langle \phi_a \mid \hat{V}^{\mathrm{NA}} + \delta\hat{V}^{\mathrm{Ha}} + \hat{V}^{\mathrm{XC}} \mid (\nabla_{i\lambda}\phi_b) R_{i\mu} \rangle + \frac{1}{2}\sum_i \sum_{ab} K_{ab} \frac{\partial T_{ab}}{\partial R_{i\lambda}} R_{i\mu} - 2\sum_i \sum_{abk} K_{ab} \langle (\nabla_{i\lambda}\phi_a) \mid \chi_k \rangle R_{i\mu} A_k \langle \chi_k \mid \phi_b \rangle - 4\sum_i \sum_{ab} \tilde{G}_{ab} \langle \phi_a \mid (\nabla_{i\lambda}\phi_b) \rangle R_{i\mu}. \tag{21}$$

It is important to note that, for linear scaling, the matrix $\tilde{G}_{ab}$ is the same matrix found in equation (18), including the effect of the variation of the electron number, while for exact diagonalisation it is simply G_{ab}.

3.3. Miscellaneous stresses

The remaining stresses do not fit easily into the two previous categories, and are given here in no particular order. The ion-ion stress within the neutral atom potential is written as follows:

$$\sigma^{\mathrm{SCC}}_{\lambda\mu} = \sum_i \frac{1}{2}\sum_j \left[\frac{Z_i Z_j}{|\mathbf{R}_i - \mathbf{R}_j|^3} \left(R_{i\lambda} - R_{j\lambda}\right) \delta_{\lambda\mu} - \int \mathrm{d}\mathbf{r} V_j^{\mathrm{Ha,PAD}}(\mathbf{r}) \frac{\partial n_i^{\mathrm{PAD}}}{\partial R_{i\lambda}} \right] \left(R_{i\mu} - R_{j\mu}\right). \tag{22}$$

Various terms in the total energy are calculated using a numerical integration on a real-space grid (the screened Hartree, exchange-correlation and neutral atom energies). There is a stress associated with the change of the Jacobian (i.e. the grid point volume):

$$\sigma^{\mathrm{Jacobian}}_{\lambda\mu} = \delta_{\lambda\mu}\left(E^{\delta\mathrm{Ha}} + E^{\mathrm{XC}} + E^{\mathrm{NA}}\right). \tag{23}$$

Similarly, since the Hartree potential is found using fast Fourier transforms, there is a stress which arises from changes of the reciprocal lattice vectors:

$$\sigma_{\lambda\mu}^{\mathrm{Ha}} = \int \mathrm{d}\mathbf{r}\delta n\left(\mathbf{r}\right)\mathrm{FT}\left[\frac{2G_\lambda G_\mu}{G^4}\tilde{\delta n}\right] \tag{24}$$

where $\tilde{\delta n}$ indicates the Fourier transform of δn, and FT[] indicates the inverse Fourier transform.

For a GGA exchange-correlation functional, which depends on the gradient of the electron density, there is an extra contribution to the stress which can be written as [36, 37]:

$$\sigma_{\lambda\mu}^{\mathrm{XC,GGA}} = \int \mathrm{d}\mathbf{r}\frac{\partial f}{\partial\nabla_\lambda n\left(\mathbf{r}\right)}\nabla_\mu n\left(\mathbf{r}\right). \tag{25}$$

When using non-linear PCC, there is a stress associated with the change of the core densities as atoms move, which can be written as:

$$\sigma_{\lambda\mu}^{\mathrm{PCC}} = \sum_i \int \mathrm{d}\mathbf{r}\nabla_{i\lambda} n_i^{\mathrm{C}}\left(\mathbf{r}\right) V_{\mathrm{XC}}\left[n\left(\mathbf{r}\right)+n^{\mathrm{C}}\left(\mathbf{r}\right)\right] R_{i\mu}. \tag{26}$$

It might be argued that this is similar to a Hellmann–Feynman stress, but the distinction is not important.

Finally, when running without self-consistency, there are stresses equivalent to the forces we have described elsewhere [29]:

$$\begin{aligned}\sigma_{\lambda\mu}^{\mathrm{Non-SCF}} = &-\int \mathrm{d}\mathbf{r}\Delta V^{\mathrm{Ha}}\left(\mathbf{r}\right)\sum_i \frac{\partial}{R_{i\lambda}} n_i^{\mathrm{PAD}} R_{i\mu} \\ &-\int \mathrm{d}\mathbf{r}\Delta n\left(\mathbf{r}\right)\mu'_{\mathrm{XC}}\left[n^{\mathrm{PAD}}+n^{\mathrm{C}}\right]\sum_i \frac{\partial}{R_{i\lambda}}\left(n_i^{\mathrm{PAD}}+n_i^{\mathrm{C}}\right) R_{i\mu}.\end{aligned} \tag{27}$$

There is also an extra Jacobian stress for the exchange and correlation:

$$\sigma^{\mathrm{XCJacobian,Non-SCF}} = \int \mathrm{d}\mathbf{r}\left(n^{\mathrm{out}}-n^{\mathrm{PAD}}\right) V_{\mathrm{XC}}\left[n^{\mathrm{PAD}}+n^{\mathrm{C}}\right]. \tag{28}$$

The Hartree stress arising from the change in reciprocal lattice vectors is identically zero for non-self-consistent calculations.

4. Tests and results

In this section we present comprehensive tests of the convergence of pressure, force and total energy with density matrix range for a variety of materials with differing properties, and then test molecular dynamics in the NPT ensemble. In all cases we compare results found with linear scaling to those found with converged exact diagonalisation. The convergence of total energy with respect to density matrix range is related to the gap of the material [38]; while there are no formal results on the convergence of forces or stresses with density matrix range, energy differences converge faster than total energies, and most linear scaling calculations rely on the fast convergence of energy *differences*, even when total energies are not converged. It is important to note that the same is true for many parameters in standard DFT calculations, e.g. k-point convergence, or plane wave cutoff in plane wave codes. For simplicity, we use a simple single zeta basis set of PAOs [24] for all calculations; the only significant effect that a larger basis set will have on the results will be if the gap is changed by the basis. Any basis set superposition errors will have a negligible effect on stress calculations in condensed phases.

All tests used Conquest v1.5 [39] which is publicly available from GitHub, and includes the stress implementation described in this paper.

4.1. Convergence tests

We consider six materials which provide a variety of types of bonding and electronic structure. The elemental semiconductors carbon, silicon and germanium are all tetrahedrally bonded, and have varying gaps (the values with the single zeta basis are not accurate, but nevertheless span an appropriate range: 5.9 eV for carbon; 2.1 eV for silicon; and 0.0 eV for germanium at the Γ point), covering behaviors from insulating, through semiconducting to metallic. We also include ionic materials, all of which

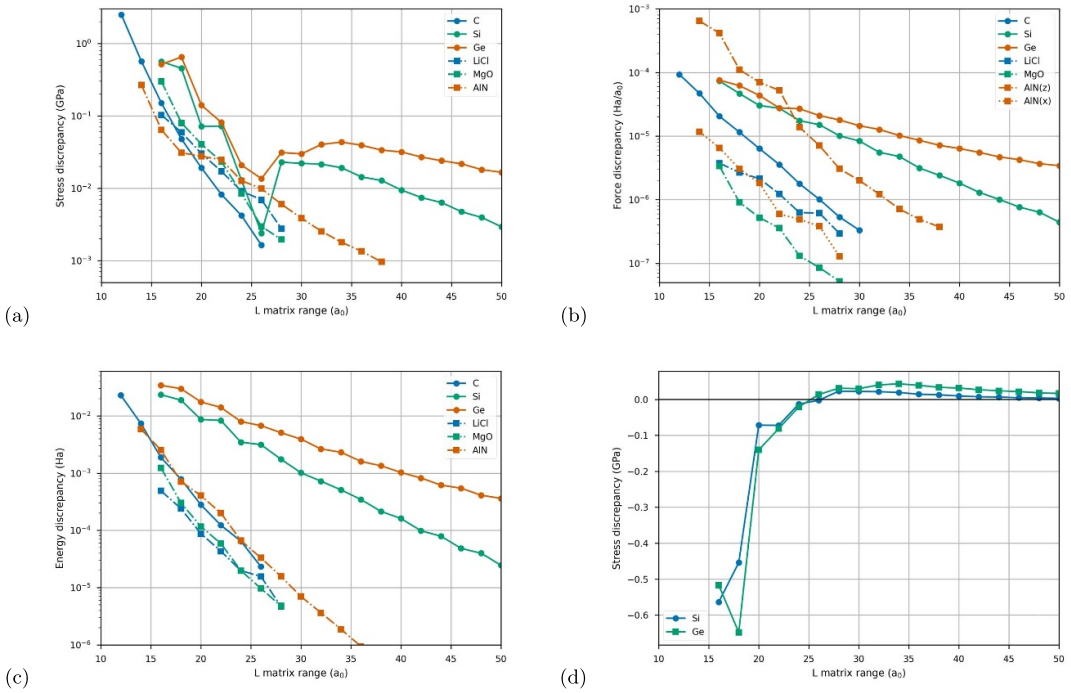


Figure 1. Absolute value of the difference between linear scaling and fully converged exact diagonalisation calculations as a function of density matrix cutoff (in a_0) for: (a) stress (in GPa); (b) force (in Ha/a_0); and (c) total energy (in Ha). (d) stress difference for Si and Ge, as in (a), on a linear scale to illustrate the cause of the dip in the stress difference curve.

have large gaps: MgO and LiCl, which are both cubic, with gaps of 5.3 eV and 7.0 eV; and AlN, which is hexagonal (wurtzite), and polar along the *c*-axis, with a gap of 3.4 eV. This variety of materials covers differences in bonding and electronic structure, and provides a stringent test of the approach. For MgO and LiCl we use the local density approximation with Troullier-Martins pseudopotentials [40], while for the other materials we use PBE [41] with Hamann pseudopotentials [28] from the PseudoDojo database [42].

In our comparisons, we use the same simulation cells, with all parameters identical except for the ground state search. In all cases, we used a perfect crystal but with one atom slightly displaced along the *c*-axis of the cell to give non-zero forces, with a lattice constant reduced by 1% from the relaxed value (for exact diagonalisation). We use a real space integration grid with a spacing of 0.2 a_0, which gives good convergence. All diagonalisation calculations used a Monkhorst–Pack grid which fully converged the total energy.

We consider three quantities: the total energy; the force; and the stress along the c-axis. In all practical circumstances we are interested in energy *differences* rather than total energies, so the stress and force graphs are much more important. The results are shown in figure 1, showing the stress in (a), the force in (b) and the total energy in (c). The unit cells of all materials apart from AlN are cubic; we have plotted the stress along the *c* axis in AlN, which is the direction of the displacement of the ion, though the convergence is similar in all directions.

Considering first the stress, we see that the discrepancy is rather small, being below 1 GPa for all materials at all density matrix ranges (except carbon with the exceptionally small density matrix range of 12 a_0) and below 0.1GPa for very reasonable density matrix ranges: 18 a_0 for the four insulators (C, LiCl, MgO and AlN), 20 a_0 for silicon, and 22 a_0 for germanium. The dip in the curve seen around 25 a_0 for Si and Ge is due to the non-monotonic convergence of the stress with density matrix range, as shown in figure 1(d); there is no fundamental reason why the stress should converge monotonically.

The force convergence is even better than the stress, with the discrepancies below 1×10^{-4} Ha/a_0 ($\simeq 5\times10^{-3}$ eV Å^{-1}) for all density matrix ranges and all materials (except AlN along a direction in the basal plane where this level requires a range of 18 a_0). This indicates that structural optimization for all elements considered here will be reliable regardless of the restriction placed on the density matrix. The final curve, showing convergence of total energy, displays the expected trends of exponential convergence, with larger gaps converging faster. Absolute energies are much less important than energy differences, which converge much faster (as seen in the stresses and forces). We note that comparison of the

Table 1. Bulk modulus in GPa calculated by fitting Birch–Murnaghan curves to energy ($B_0^{(E)}$) and pressure ($B_0^{(P)}$) for the six materials, for linear scaling ($R_L = 18a_0$ for C, LiCl, MgO, AlN, $R_L = 20a_0$ for Si and $R_L = 22a_0$ for Ge) and exact diagonalisation.

	C	Si	Ge	LiCl	MgO	AlN
O(N) $B_0^{(E)}$	391.8	72.5	46.0	39.8	187.3	182.1
Diag $B_0^{(E)}$	391.8	71.3	46.9	39.6	185.5	181.7
O(N) $B_0^{(P)}$	395.6	71.9	46.2	39.3	185.6	180.9
Diag $B_0^{(P)}$	395.5	70.5	47.9	39.1	185.4	180.4

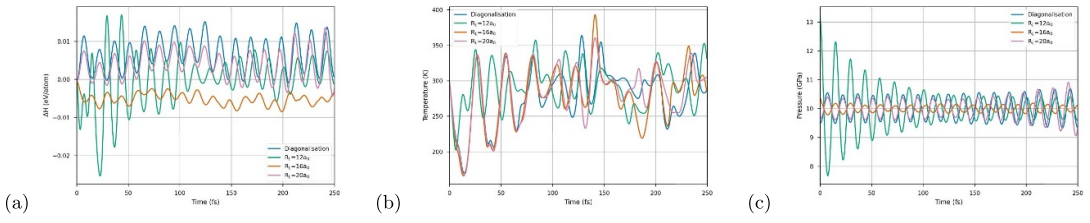


Figure 2. Characterization of the effect of density matrix range on NPT molecular dynamics. (a) Deviation of conserved quantity; (b) temperature and (c) pressure variation. In all cases results for full diagonalisation are compared to three density matrix ranges (12, 16 and 20 a_0).

analytic stresses presented here with numerical stresses found from the energy change resulting from a small volume change are in excellent agreement.

As a further test of the stress calculation, we evaluate the bulk modulus for all materials by fitting to seven point curves in both the energy (as is standard for DFT calculations) and the pressure on the simulation cell (which tests the stress explicitly). For the linear scaling calculations, we use the same density matrix range identified above where the stress error is less than 0.1 GPa ($18a_0$ for C, LiCl, MgO and AlN; $20\,a_0$ for Si and $22\,a_0$ for Ge). We found that rather than using a fixed density matrix range for each point on the binding energy curve, better convergence is obtained by scaling the density matrix range with simulation cell size [43]. The results are given in table 1, and show excellent agreement.

4.2. Molecular dynamics tests

We now turn to a practical application of the calculated stress: isobaric-isothermal molecular dynamics. We have already demonstrated NVE molecular dynamics with linear scaling DFT on systems up to 32 678 atoms [35], using the extended Lagrangian Born–Oppenheimer (XL-BOMD) approach [44]. In that work, we showed that the total energy was well conserved, with small fluctuations (no more than 1 meV $atom^{-1}$ even for a small density matrix range of 14 a_0) which reduced with increasing density matrix range. We have also demonstrated dynamics under the NVT ensemble [45], again showing stable dynamics with good conservation. Here, we show that stable linear scaling molecular dynamics is possible for the NPT ensemble, and characterize the behavior with density matrix range. We choose a temperature of 300 K and a pressure of 10 GPa for a sample of bulk silicon. We are particularly interested in the effects of the density matrix range on fidelity of the dynamics: both the stability and conservation of the simulations, and how closely the full diagonalisation dynamics can be followed.

In figure 2 we consider the case where we used identical simulation settings for all tests, including the same starting seed for the pseudo-random number generator and starting simulation cell size. We note that the initial pressures in these cases differ with density matrix range (as seen in figure 1), with a difference to exact diagonalisation of less than 0.1 GPa at $R_L = 20a_0$. As the density matrix range increases, the linear scaling dynamics converge towards the exact diagonalisation dynamics; in all cases, we see that the conserved quantity does not drift, and the pressure and temperature are maintained at their set point.

As would be expected, the smaller density matrix ranges show more differences in the detailed dynamics to the exact diagonalisation results, while the $R_L = 20\,a_0$ results follow the exact diagonalisation results closely. In particular, the pressure fluctuations are out of phase with the exact diagonalisation results, and the conserved quantity follows a somewhat different path (though with the same underlying frequency of oscillation). The key question to understand in terms of fidelity of dynamics is whether this is purely due to the difference in initial pressure, or also due to differences in forces;

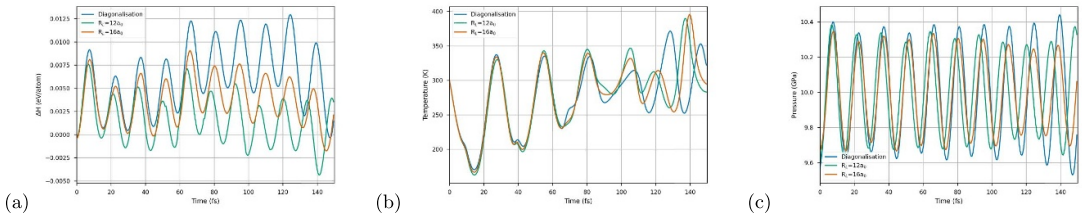


Figure 3. Comparison of NPT molecular dynamics starting from the same initial pressure for diagonalisation and linear scaling calculations. (a) Deviation of conserved quantity; (b) temperature and (c) pressure variation. In all cases, results for full diagonalisation are compared to two density matrix ranges (12 and 16 a_0).

from the results in figure 1(b) we would expect it to be almost entirely from pressure. We investigated dynamics for short density matrix ranges (R_L = 12 and 16 a_0) with simulation cell sizes adjusted to give the same initial pressure as in the exact diagonalisation simulation (to within 0.1 GPa). The results are shown in figure 3.

We see that for the first hundred femtoseconds of dynamics the short density matrix range simulations follow the exact diagonalisation trajectories extremely closely. The increase in difference over time is an inevitable result of slight variations in dynamics. The result of these simulations is extremely encouraging for large scale, long-time DFT dynamics: we see that high quality simulations can be achieved using very modest density matrix ranges. Comparing diagonalisation and O(N) calculations [46] we find a drift of less than 0.001 eV ps^{-1} $atom^{-1}$ for simulations spanning multiple picoseconds.

5. Conclusions

We have shown how stress can be calculated in the context of the local orbital DFT code CONQUEST, both in terms of exact diagonalisation and linear scaling operation. Tests of the convergence of the stress calculated with linear scaling to the exact diagonalisation result show that relatively modest density matrix ranges are required for excellent agreement, with all materials converged to within 0.1 GPa with a range of 20 a_0. Tests of NPT dynamics show no drift in the conserved quantity, and stable dynamics over meaningful timescales. Moreover, adjusting the starting simulation cell size so that the initial pressures of both linear scaling and exact diagonalisation are the same allows us to reproduce the exact dynamics over 100 fs for very small ranges, as low as 12 a_0 for silicon.

Our results demonstrate that the full range of molecular dynamics ensembles can be used with linear scaling DFT methods with no loss of accuracy in the dynamics of the system, even with modest density matrix ranges. This opens the prospect of very large scale dynamics calculations with full DFT accuracy. The remaining questions for linear scaling MD simulations concern basis set size and overall efficiency. Since the support functions in CONQUEST are non-orthogonal, we require the inverse of the overlap matrix for efficient calculations [32, 47], but with linear scaling time. At present, we find an approximate, short range inverse matrix using Hotelling's method, though this approach performs poorly for larger PAO basis sets as the overlap matrix becomes increasingly ill-conditioned. The lack of an inverse overlap matrix potentially restricts the basis size that can be used, though the use of the alternative blip basis sets [23, 30] and the on-site support function approach outlined recently [7] offer ways forward here. The question of efficiency is key to long timescale MD runs. We already use the extended Lagrangian approach to molecular dynamics [44] to ensure energy conservation, though this can require more iterations to find the ground state than simple reuse of the density matrix; extensions of the extended Lagrangian approach that require no self-consistency cycles [48] may help with efficiency. Once these questions have been addressed, the route to very large scale, long DFT molecular dynamics runs is open.

Acknowledgments

This research was partly carried out using the high performance computing cluster in the London Center for Nanotechnology. The authors acknowledge the use of the UCL Kathleen High Performance

Computing Facility (KathleenUCL), and associated support services, in the completion of this work. We are grateful for computational support from the UK Materials and Molecular Modeling Hub, which is partially funded by EPSRC (EP/T022213/1, EP/W032260/1 and EP/P020194/1), for which access was obtained via the UKCP consortium and funded by EPSRC grant ref EP/X035891/1.

Data availability statement

The data that support the findings of this study are openly available at the following URL/DOI: https://doi.org/10.5281/zenodo.21262374 [49].

Author contributions

Shereif Y Mujahed 0000-0002-7121-073X
Formal analysis (equal), Methodology (equal), Software (equal), Writing – original draft (equal)

Tsuyoshi Miyazaki 0000-0003-3534-4404
Conceptualization (equal), Supervision (equal), Writing – review & editing (equal)

David R Bowler 0000-0001-7853-1520
Conceptualization (equal), Formal analysis (equal), Investigation (equal), Methodology (equal), Software (equal), Supervision (equal), Writing – original draft (equal), Writing – review & editing (equal)

References

[1] Martin R M 2020 *Electronic Structure: Basic Theory and Practical Methods* 2nd edn (Cambridge University Press) (https://doi.org/10.1017/9781108555586)
[2] Carnimeo I *et al* 2023 Quantum espresso: One further step toward the exascale *J. Chem. Theory Comput.* **19** 6992–7006
[3] Ratcliff L E *et al* 2020 Flexibilities of wavelets as a computational basis set for large-scale electronic structure calculations *J. Chem. Phys.* **152** 194110
[4] García A *et al* 2020 Siesta: Recent developments and applications *J. Chem. Phys.* **152** 204108
[5] Prentice J C A *et al* 2020 The onetep linear-scaling density functional theory program *J. Chem. Phys.* **152** 174111
[6] Kühne T D *et al* 2020 Cp2k: an electronic structure and molecular dynamics software package - quickstep: Efficient and accurate electronic structure calculations *J. Chem. Phys.* **152** 194103
[7] Nakata A *et al* 2020 Large scale and linear scaling DFT with the CONQUEST code *J. Chem. Phys.* **152** 164112
[8] Nakata A, Bowler D R and Miyazaki T 2022 Large-scale DFT methods for calculations of materials with complex structures *J. Phys. Soc. Jpn.* **91** 091011
[9] Bowler D R and Miyazaki T 2010 Calculations on millions of atoms with density functional theory: linear scaling shows its potential *J. Phys.: Condens. Matter* **22** 074207
[10] Arita M, Arapan S, Bowler D R and Miyazaki T 2014 Large-scale DFT simulations with a linear-scaling DFT code CONQUEST on K-computer *J. Adv. Simul. Sci. Eng.* **1** 87–97
[11] Miyazaki T, Bowler D R, Choudhury R and Gillan M J 2004 Atomic force algorithms in density functional theory electronic-structure techniques based on local orbitals *J. Chem. Phys.* **121** 6186–94
[12] Pulay P 1969 *Mol. Phys.* **17** 197
[13] Feibelman P J 1991 Pulay-type formula for surface stress in a local-density-functional, linear combination of atomic orbitals, electronic-structure calculation *Phys. Rev. B* **44** 3916–25
[14] Soler J M, Artacho E, Gale J D, García A, Junquera J, Ordejón P and Sánchez-Portal D 2002 The SIESTA method for ab initio order-N materials simulation *J. Phys.: Condens. Matter* **14** 2745–70
[15] Sharma A, Hamel S, Bethkenhagen M, Pask J E and Suryanarayana P 2020 Real-space formulation of the stress tensor for o(n) density functional theory: application to high temperature calculations *J. Chem. Phys.* **153** 034112
[16] Nielsen O H and Martin R M 1983 First-principles calculation of stress *Phys. Rev. Lett.* **50** 697–700
[17] Nielsen O H and Martin R M 1985 Quantum-mechanical theory of stress and force *Phys. Rev. B* **32** 3780–91
[18] Ozaki T and Kino H 2005 Efficient projector expansion for the ab initio lcao method *Phys. Rev. B* **72** 045121
[19] We have a pseudo-atomic density, since we use a pseudopotential and solve for pseudo-atomic orbitals (PAOs)
[20] Harris J 1985 *Phys. Rev. B* **31** 1770
[21] Foulkes W and Haydock R 1989 *Phys. Rev. B* **39** 12520
[22] Kohn W and Sham L J 1965 *Phys. Rev.* **140** A1133
[23] Hernández E, Gillan M J and Goringe C M 1996 Linear-scaling density-functional-theory technique: The density-matrix approach *Phys. Rev. B* **53** 7147–57
[24] Bowler D R, Baker J S, Poulton J T L, Mujahed S Y, Lin J, Yadav S, Raza Z and Miyazaki T 2019 Highly accurate local basis sets for large-scale DFT calculations in conquest *Jpn. J. Appl. Phys.* **58** 100503
[25] Bowler D R and Miyazaki T 2012 $\mathcal{O}$(N) methods in electronic structure calculations *Rep. Prog. Phys.* **75** 036503
[26] Goedecker S 1999 Linear scaling electronic structure methods *Rev. Mod. Phys.* **71** 1085
[27] Louie S G, Froyen S and Cohen M L 1982 *Phys. Rev. B* **26** 1738
[28] Hamann D R 2013 Optimized norm-conserving vanderbilt pseudopotentials *Phys. Rev. B* **88** 085117

[29] Torralba A S, Bowler D R, Miyazaki T and Gillan M J 2009 Non-self-consistent Density-Functional Theory Exchange-Correlation Forces for GGA Functionals *J. Chem. Theory Comput.* **5** 1499
[30] Bowler D R, Miyazaki T and Gillan M J 2002 Recent progress in linear scaling *ab initio* electronic structure techniques *J. Phys.: Condens. Matter* **14** 2781–98
[31] Li X-P, Nunes R W and Vanderbilt D 1993 Density-matrix electronic-structure method with linear system-size scaling *Phys. Rev. B* **47** 10891–4
[32] Nunes R W and Vanderbilt D 1994 Generalization of the density-matrix method to a nonorthogonal basis *Phys. Rev. B* **50** 17611–4
[33] Bowler D R and Gillan M J 1999 Density matrices in O(N) electronic structure calculations: theory and applications *Comput. Phys. Commun.* **120** 95–108
[34] Palser A H R and Manolopoulos D E 1998 Canonical purification of the density matrix in electronic-structure theory *Phys. Rev. B* **58** 12704–11
[35] Arita M, Bowler D R and Miyazaki T 2014 Stable and efficient linear scaling first-principles molecular dynamics for 10,000+ atoms *J. Chem. Theory Comput.* **10** 5419
[36] Corso A D and Resta R 1994 Density-functional theory of macroscopic stress: Gradient-corrected calculations for crystalline se *Phys. Rev. B* **50** 4327–31
[37] Balbás L C, Martins J L and Soler J M 2001 Evaluation of exchange-correlation energy, potential and stress *Phys. Rev. B* **64** 165110
[38] Prodan E and Kohn W 2005 Nearsightedness of electronic matter *Proc. Natl Acad. Sci. USA* **102** 11635
[39] Conquest v1.5 2026 (available at: https://github.com/OrderN/CONQUEST-release) (24 September 2026)
[40] Troullier N and Martins J L 1991 Efficient pseudopotentials for plane-wave calculations *Phys. Rev. B* **43** 1993–2006
[41] Perdew J P, Burke K and Ernzerhof M 1996 Generalized gradient approximation made simple *Phys. Rev. Lett.* **77** 3865–8
[42] van Setten M J, Giantomassi M, Bousquet E, Verstraete M J, Hamann D R, Gonze X and Rignanese G M 2018 The pseudodojo: training and grading a 85 element optimized norm-conserving pseudopotential table *Comput. Phys. Commun.* **226** 39–54
[43] This ensures that the number of non-zero density matrix elements is constant across all calculations, in close analogy to similar calculations performed with a plane wave basis set, which generally use a constant number of plane waves
[44] Niklasson A M N 2008 *Phys. Rev. Lett.* **100** 123004
[45] Hirakawa T, Suzuki T, Bowler D R and Miyazaki T 2017 Canonical-ensemble extended Lagrangian Born–Oppenheimer molecular dynamics for the linear scaling density functional theory *J. Phys.: Condens. Matter* **29** 405901
[46] To simplify this comparison, we exclude the thermostat energy so that any difference is solely due to the electronic structure solver
[47] Bowler D R, Bush I J and Gillan M J 2000 Practical methods for *ab initio* calculations on thousands of atoms *Int. J. Quant. Chem.* **77** 831–42
[48] Souvatzis P and Niklasson A M N 2014 First principles molecular dynamics without self-consistent field optimization *J. Chem. Phys.* **140** 044117
[49] Mujahed S Y, Miyazaki T and Bowler D R 2026 *Zenodo* (https://doi.org/10.5281/zenodo.21262374)